

Singularity-Aware Motion Planning for Multi-Axis Additive Manufacturing

Tianyu Zhang¹, Xiangjia Chen², Guoxin Fang^{3,1}, Yingjun Tian¹ and Charlie C.L. Wang^{1†}, *Senior Member, IEEE*

Abstract—Multi-axis additive manufacturing enables high flexibility of material deposition along dynamically varied directions. The Cartesian motion platforms of these machines include three parallel axes and two rotational axes. Singularity on rotational axes is a critical issue to be tackled in motion planning for ensuring high quality of manufacturing results. The highly nonlinear mapping in the singular region can convert a smooth toolpath with uniformly sampled waypoints defined in the model coordinate system into a highly discontinuous motion in the machine coordinate system, which leads to over-extrusion / under-extrusion of materials in filament-based additive manufacturing. The problem is challenging as both the maximal and the minimal speeds at the tip of a printer head must be controlled in motion. Moreover, collision may occur when sampling-based collision avoidance is employed. In this paper, we present a motion planning method to support the manufacturing realization of designed toolpaths for multi-axis additive manufacturing. Problems of singularity and collision are considered in an integrated manner to improve the motion therefore the quality of fabrication.

I. INTRODUCTION

ADDITIVE manufacturing (AM) has shown significant impact on a variety of industrial applications with its capability in agile fabrication of products with complex geometry [1], [2]. The conventional AM setup always conducts three-axis motion and accumulates material in planar layers along the z-axis. Although this simplification can reduce the cost of hardware system and the complexity of software, it also brings the problems of weak mechanical strength [3], additional supporting structure under overhang [4] and staircase artifacts on the surface [5].

In recent years, AM systems including multi-axis motion have been developed to overcome the drawbacks of planar layer-based material deposition. Material deposition can be conducted along the normal of curved surface in these systems so that they enable advanced functions such as support-free or supportless printing [6]–[11], strength enhancement [12], [13] and surface quality improvement [14], [15]. Different from planar-layer based AM, the *multi-axis additive manufacturing* (MAAM) system not only requires advanced algorithms to generate toolpaths on curved layers but also brings in the challenge of realizing complicated toolpaths on hardware by motion planning.

¹T. Zhang, G. Fang, Y. Tian and C.C.L. Wang are with the Department of Mechanical, Aerospace and Civil Engineering, University of Manchester, UK

²X. Chen is with the Department of Mechanical and Automation Engineering, Chinese University of Hong Kong, (CUHK) China.

³G. Fang is also a PhD student with the Faculty of Industrial Design, Delft University of Technology, The Netherlands.

This work was partially supported by HKSAR RGC General Research Fund: 14202219 when the authors worked at CUHK.

[†]Corresponding Author: changling.wang@manchester.ac.uk

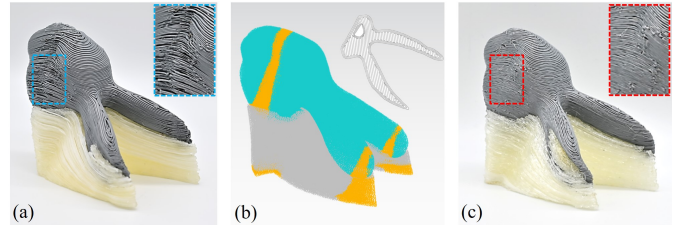


Fig. 1. Bunny models fabricated with curved layers by MAAM with rotational tilting table. (a) Surface artifacts (circled region) caused by not well-planned motion. (b) Waypoints in singular region are shown in yellow color. (c) The surface quality improvement after singularity-aware motion planning.

A. Problem of Motion Planning in MAAM

Without loss of the generality, a toolpath for MAAM can be represented as a set of waypoints containing both position and orientation information represented in the *work-piece coordinate system* (WCS). The waypoints are uniformly sampled on the toolpath to indicate the desired movement of nozzle during the process of material deposition in a speed with less variation. Each waypoint on a toolpath is transferred into the *machine coordinate system* (MCS) by inverse kinematics. However, the mapping between WCS and MCS is nonlinear, especially in the region where the normal direction is close to vertical. This issue has been studied in multi-axis *computer numerical control* (CNC) milling as singularity (Sec. II-C) where solutions has been developed in prior research (see Sec. I-B). However, the existing CNC solutions cannot be directly applied to MAAM. The reason is threefold.

- **Continuous Motion:** The filament extrusion during printing process should not be broken; otherwise, both the surface quality and the mechanical strength of 3D printed models will be influenced (ref. [13], [16]) – see also the illustration given in Fig.1.
- **Speed Constraints:** The feedrate of material deposition can only be stably controlled by the extruder in a range $[f_{\min}, f_{\max}]$, which is limited by its working principle in physics. As a consequence, motion speed at the tip of a printer head needs to be well controlled within a corresponding range – i.e., with both the lower and the upper bounds. To ensure a speed larger than the lower bound becomes challenging in the singular region as it may require a fast rotation that is already beyond the capability of a motor’s maximal speed. Details will be discussed in Sec. III-B.
- **Collision-free:** Collision avoidance in MAAM is more critical as the working surfaces in freeform shape can be highly complex with many concave regions. When tuning

waypoints’ normals to optimize motion, collision detection should be systematically integrated in the routine of optimization.

In this work, we present a singularity-aware motion planning pipeline for MAAM, and it is a variant of sampling-based motion planning. Both singularity and collision are considered in an integrated way. By our approach, the collision-free motion of a given toolpath will be generated to optimize the motion speed at the printer head¹ (i.e., falling in the range determined by the feedrates of material extrusion that can be realized). As a result, the quality of physical fabrication can be significantly improved (see Fig.1 for an example). To the best of our best knowledge, no prior work in CNC literature has directly controlled the minimal speed of motion on a tool.

B. Related work

We review the related work of motion planning on multi-axis machines in both CNC milling and 3D printing.

1) *Motion planning in multi-axis CNC*: For subtractive manufacturing, the singularity and collision issues for multi-axis CNC system have been studied for decades. To deal with singularity, singular cone region was introduced in [18]. Sorby et al. [19] provided a singularity solution for CNC machine with a non-orthogonal rotary table. In multi-axis CNC machining, lifting and re-positioning the cutter [20] is a possible and intuitive solution to solve the singularity issues. However, MAAM has strict requirement on the continuity of motion. This method of retraction cannot be applied here. Boz et al. [21] solved the winding problem and considered the dual IK solutions at each waypoint; however, they did not consider the smoothness of normal variation in singular region. Yang et al. [22] used spline curves in fifth degree to improve the continuous of rotation in the singular region, which however did not utilize the dual IK solutions to decrease the variation of axial motion. Based on the real-time feedback of joint angles, My and Bohez [23] proposed an analytical scheme for identifying and avoiding singular configurations. Grandguillaume et al. [24] solved the singularity problem by controlling the waypoints to going through the singular region while respecting the maximal velocity, acceleration and jerk on the rotary axes. Collision-free is not directly considered in their solution of singularity. There are also researches with focus on generating a collision-free toolpath. Wang and Tang [25] conducted a method to guarantee the collision-free and angular-velocity compliance in the CNC machining process. Potential field is employed in [26] to find a feasible region away from the obstacle when the collision of milling tool is detected. Xu et al. [27] proposed a kinematic performance oriented smoothing method to conduct collision avoidance. However, more complex shapes and larger tools make collision detection more complicated in MAAM, and

¹In the singular region, little variation of orientation in WCS between two neighboring waypoints could result in large rotational movement [17] in MCS (e.g., C-axis). This problem of slow motion at the printer head can only be solved by either adjusting the orientations of waypoints (our method) or using a fast enough motor (may cause some problem of dynamic stability). It cannot be solved by adding more waypoints into the toolpath.

meanwhile collision detection and singularity optimization are coupled together.

2) *Motion planning in AM and MAAM*: For the traditional planar-layer based AM, only translation motion is involved in the manufacturing process and it is realized by Cartesian or Delta structures. This machine configuration naturally avoids collision issue and makes the control task of motion easier to solve. Material deposition at sharp features [28], [29] and the continuity of filament extrusion [30] have been well studied for planar-layer based AM. A more comprehensive survey of motion and toolpath planning in AM can be found in [31]. When more *degrees of freedom* (DOFs) are introduced into the material processing, the complexity of motion planning increases sharply for multi-axis machines due to the kinematic redundancy and the collision issues. As a flexible motion platform, robotic arms have been employed to realize multi-axis motion for 3D printing (see [32] for a survey). Prior works [9], [33], [34] have provided the smooth path planning and feed-rate control for robot-assisted MAAM system. Huang et al. [35] present an optimization-based planning method for robot-assisted frame structure of 3D printing, which finds feasible fabrication sequence to avoid collision. Bhatt et al. [6] adopted a neural network-based scheme to improved both the accuracy and the time lag error for fabricating more accurate parts. Dai et al. [36] developed an algorithm to preserve discrete time constraints when optimizing jerk behavior for the motion of robotic arm. However, there is less work focusing on motion planning under the speed limitation in singularity region for Cartesian-type multi-axis printers. These machine structure (as shown in Fig.2) are more commonly used for MAAM or hybrid machining as it can generally provide motion with higher precision.

C. Our approach

This following contributions are made in this paper:

- We present a sampling-based motion planning algorithm to generate a singularity-aware, smooth and collision-free motion by adjusting nozzle orientations of waypoints on a given toolpath, where the coupled problem of collision and singularity are solved systematically.
- Our algorithm optimizes the motion of machine to satisfy the required range of speeds on the nozzle movement that is derived from the speed limits of material extrusion, and hence improves the surface quality of fabricated models in the singular regions.

Our motion planning method is general, which can support MAAM systems in different machine configurations. The effectiveness of our motion planning is demonstrated by the quality of fabrication results and can also be observed from the supplementary video.

II. MOTION PLANNING IN MAAM: PROBLEM ANALYSIS

In the process of MAAM, the nozzle of printer head moves along designed toolpaths to align materials, where each toolpath \mathcal{L} is usually represented by a set of waypoints with both position and orientation information. We remark a single waypoint as $\mathbf{x} = [\mathbf{p}, \mathbf{n}] \in \mathbb{R}^6$, where $\mathbf{p} = [p_x, p_y, p_z]$

TABLE I
INVERSE KINEMATICS OF MAAM SYSTEMS IN THREE DIFFERENT MACHINE CONFIGURATIONS

	Configuration I (Fig. 2(a)): rotational table and tilting head	Configuration II (Fig. 2(b)): rotational and tilting extrusion head	Configuration III (Fig. 2(c)): rotational and tilting platform
B/C	$B = \pm a \cos(n_z), \quad C = -atan2(n_y/n_x) \pm \pi H(B)$		
X	$p_x \cos C - p_y \sin C + d \sin B$	$p_x + r \sin C + h \cos C \sin B$	$p_x \cos B \cos C - p_y \cos B \sin C + p_z \sin B$
Y	$-p_x \sin C - p_y \cos C$	$p_y - r \cos C + h \sin C \sin B + r$	$p_x \sin C + p_y \cos C$
Z	$p_z - d(1 - \cos B)$	$p_z + h \cos B - h$	$p_y \sin B \sin C - p_x \sin B \cos C + p_z \cos B$
A/C	$A = \pm a \cos(n_z), \quad C = -atan2(n_x/n_y) \pm \pi H(A)$		
X	$-p_x \cos C + p_y \sin C$	$p_x - r \cos C + h \sin C \sin A + r$	$p_x \cos C - p_y \sin C$
Y	$p_x \sin C + p_y \cos C - d \sin A$	$p_y - r \sin C - h \cos C \sin A$	$p_x \cos A \sin C + p_y \cos A \cos C - p_z \sin A$
Z	$p_z - d(1 - \cos A)$	$p_z + h \cos A - h$	$p_x \sin A \sin C + p_y \sin A \cos C + p_z \cos A$

* d is the distance between the tip of nozzle and the B-axis, h is the distance between the tip of nozzle and the intersection of B and C axes, and r defines the distance between the tip of nozzle and the C-axis. All these symbols have been illustrated in Fig. 2.

and $\mathbf{n} = [n_x, n_y, n_z]$ represent the position and the nozzle orientation respectively. Note that \mathbf{n} is a normalized vector in the rest of our paper. In this section, we first study the problem of motion requirement caused by the control of material extrusion. The solution of *inverse kinematics* (IK) for three different machine configurations are then presented. Lastly, the coupled issues of singularity and collision are discussed.

A. Extrusion Control and Motion Requirement

For most systems of multi-axis motion, the dynamic control of extra DOF such as the motor for material extrusion can be well synchronized with the axial motions. However, the speed of material extrusion is not only limited by the motor of extruder but also many other factors (e.g., the diameter of filaments and the hysteresis property of materials). There is a bounded range of material extrusion speed which could be obtained from experiment as $[f_{min}, f_{max}]$. For MAAM machine, the layer thickness and the toolpath width are dynamically changed. We then estimate the amount of material extrusion between \mathbf{x}_i and \mathbf{x}_{i+1} as

$$\Delta E = \frac{k}{4}(T(\mathbf{x}_i) + T(\mathbf{x}_{i+1}))(W(\mathbf{x}_i) + W(\mathbf{x}_{i+1}))\|\mathbf{p}_{i+1}\mathbf{p}_i\| \quad (1)$$

where ΔE denotes the volume of extrusion between two waypoints \mathbf{x}_i and \mathbf{x}_{i+1} . $T(\cdot)$ and $W(\cdot)$ are the layer thickness and the toolpath width at a waypoint, and k is a machine-related coefficient that can be obtained by calibration. The minimally required time and the maximally allowed time to travel between \mathbf{x}_i and \mathbf{x}_{i+1} can be derived as $[t_{min}, t_{max}] = [\Delta E/f_{max}, \Delta E/f_{min}]$.

Based on the above analysis, the motion speed v at the tip of a printer head should fall in the following range as $v \in [v_{min}, v_{max}]$ to achieve a stable material extrusion:

$$[v_{min}, v_{max}] = \left[\frac{f_{min}\|\mathbf{p}_{i+1}\mathbf{p}_i\|}{\Delta E}, \frac{f_{max}\|\mathbf{p}_{i+1}\mathbf{p}_i\|}{\Delta E} \right]. \quad (2)$$

The upper bound v_{max} is imposed to avoid under-extrusion that can be satisfied by inserting more sample points between two neighboring waypoints. Moreover, the lower bound v_{min} is to prevent over-extrusion, which cannot always be achieved when the motion trajectory passing through the singular region. This will be analyzed below and can be achieved by our motion planning algorithm.

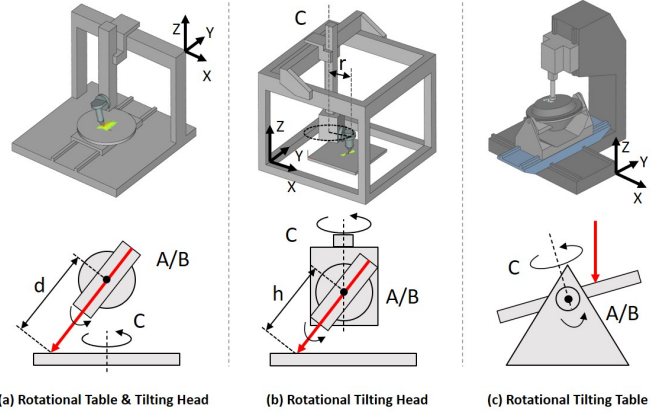


Fig. 2. Three different configurations of parallel-based multi-axis motion platforms, where the top row shows their application in MAAM systems. Red arrows in the bottom row are used to denote the nozzle of printer head.

B. Kinematics of Parallel-based Multi-Axis Setups

The essential step of motion planning is to compute the forward / inverse kinematics of a machine used in MAAM, which actually defines the mapping between WCS and MCS. In our work, three different parallel-based multi-axis setups are employed to realize linear and rotational movement of the nozzle (see Fig. 2 for the illustration).

Forward kinematics of machines in these configurations is straightforward. Here we only discuss IK solutions as the singularity problem is caused by it. For a given waypoint \mathbf{x} , we can obtain its IK solution on all the three configurations with B and C axes as

$$B = \pm a \cos(n_z), \quad C = -atan2\left(\frac{n_y}{n_x}\right) \pm \pi H(B), \quad (3)$$

where $H(\cdot)$ is the Heaviside step function. Note that for the configuration with B-axis being replaced by A axial rotation, the IK solution can be obtained by replacing n_y/n_x with n_x/n_y in Eq.(3), which gives

$$A = \pm a \cos(n_z), \quad C = -atan2\left(\frac{n_x}{n_y}\right) \pm \pi H(A). \quad (4)$$

The corresponding solutions for linear axis motion (i.e., X, Y and Z) are listed in Table I.

C. Issue of Singularity

We now analyze the reason of singularity and also the coupled winding issue in the solution of C-axis.

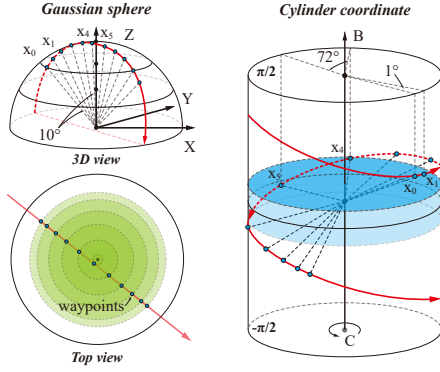


Fig. 3. Illustration of the singularity caused by the highly nonlinear mapping of IK solutions.

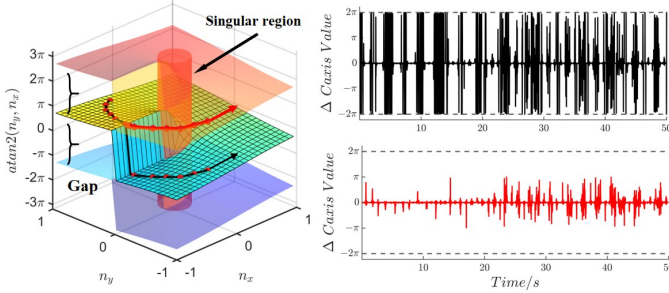


Fig. 4. Motion gap of C-axis is caused by the function $\text{atan2}()$, and the singular region is visualized as the red cylinder (left). The sharp jumps on C-axis (right-top) can be reduced by considering the winding solution (right-bottom), where the corresponding solutions are also shown in the left as red and black curves.

Directly using the IK solution (Eqs.3 and 4) will result in enormous change of rotational angle when the orientation \mathbf{n} of a waypoint is nearly parallel to Z-axis in WCS. For example as shown in Fig.3, the IK solution can map a trajectory with uniform variation in orientations (i.e., 10° between any two neighboring waypoints \mathbf{x}_i and \mathbf{x}_{i+1}) into a motion with highly non-uniform angle change on the C-axis – e.g., 72° between \mathbf{x}_4 and \mathbf{x}_5 while there is only 1° between \mathbf{x}_0 and \mathbf{x}_1 . This is caused by the nonlinear mapping introduced by the $\text{atan2}(\cdot)$ function. The region of configurations with the angle to Z-axis less than α is defined as the singular region (e.g., the red cylindrical region shown in the left of Fig. 4), where α is a machine-oriented coefficient that can be tuned by experiment [19]. When the angle change between two neighboring waypoints on C-axis is too large, the motor used for C-axis may not be able to provide the speed that is fast enough to result in the speed $v > v_{\min}$ at the tip of printer head. To solve this problem, we adjust the orientations of waypoints in the singular region to control the maximal angle difference between neighboring waypoints.

Considering the property of $\text{atan2}(\cdot)$ in Eq.(3), there are discontinuity at $\pm\pi$, which brings sharp jump if $n_x < 0$ and n_y changes its sign between neighbor waypoints (as shown in the left of Fig. 4). Meanwhile, there are multiple solutions of B- and C-axis in Eq. 3. Especially, if the range limitation of C-axis within $[-\pi, +\pi]$ is released, periodic solutions on C-axis can be employed to remove the sharp jump by considering the continuity between configurations of two neighboring waypoints (see the right of Fig. 4). However, winding solutions

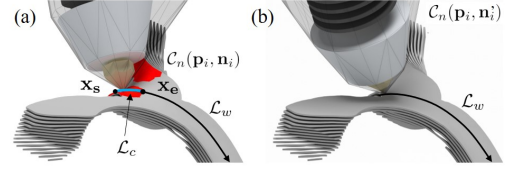


Fig. 5. Eliminating collision by local orientation adjustment. (a) A direction of extruder that will lead to collision (region shown in red). (b) Collision is eliminated after orientation adjustment.

cannot solve the aforementioned issue of singularity.

In the following section, we present a motion planning method to solve the problem of singularity by adjusting the orientation of waypoints falling in the singular region. The goal is to ensure the moving speed v between two waypoints always be feasible within the range $[v_{\min}, v_{\max}]$. Moreover, collision should be avoided when changing the orientations of waypoints. Details are discussed in the following section.

III. SINGULARITY-AWARE MOTION PLANNING

In this section, we present our motion planning method considering both the singularity and the collision issues. A sampling-based strategy is employed here. Every waypoint is converted into one or more points in the machine configuration space MCS, where some waypoints' orientations will be slightly adjusted. The final trajectory of motion is determined as an optimal path on the graph formed by using these configuration points as nodes, where the total angle variation on B- and C-axes is minimized.

A. Collision elimination by orientation adjustment

When using the prior curved-layer slicer [7], [13] to generate the toolpaths for MAAM, the initial orientations of waypoints are computed by the normals of local surface according to the heuristic of applying a locally vertical material adhesion. As only local shape is considered, these initial assignments of waypoints cannot ensure the orientation smoothness throughout the whole toolpath \mathcal{L} . Collision also occurs at some local regions (see Fig. 5(a) for an illustration). Laplacian based smoothing can be applied to the orientations of waypoints to enhance the smoothness of a toolpath but it can also make collision-free waypoints become collided, which will be further processed by the method introduced below.

Collision detection is conducted by modeling a convex-hull of the printer head as \mathcal{C} , which is axial symmetry. For a waypoint $\mathbf{x}_i \in \mathcal{L}$, we apply rigid transformation to \mathcal{C} so that the nozzle's tip is located at the \mathbf{p}_i and the rotational axis of \mathcal{C} is aligned with \mathbf{n}_i . The transformed convex-hull is denoted by $\mathcal{C}(\mathbf{p}_i, \mathbf{n}_i)$. The collision-indication function $\Gamma(\cdot)$ can be evaluated by

$$\Gamma(\mathbf{x}_i) = \begin{cases} 0, & \mathcal{C}_n(\mathbf{p}_i, \mathbf{n}_i) \cap \mathcal{M}_i \cap \mathcal{P} = \emptyset \\ 1, & \text{otherwise} \end{cases}, \quad (5)$$

where \mathcal{P} denotes the platform and \mathcal{M}_i represents the part of model already printed before \mathbf{x}_i .

We can segment the (smoothed) toolpath \mathcal{L} into collided region \mathcal{L}_c and collision-free region \mathcal{L}_w . For every waypoint $\mathbf{x}_i = (\mathbf{p}_i, \mathbf{n}_i)$ in \mathcal{L}_c , we generate k variants of \mathbf{x}_i as $\tilde{\mathbf{x}}_i^j =$

$(\mathbf{p}_i, \mathbf{n}_i^j)$ with $j = 1, \dots, k$ by randomly sampling \mathbf{n}_i^j on the Gaussian sphere around the point \mathbf{n}_i with $\mathbf{n}_i^j \cdot \mathbf{n}_i \geq \cos \beta$. The value of β is used to control the maximally allowed change in orientation (e.g., $\beta = 45^\circ$ is employed in our implementation). The collision check is applied to every variant and only the collision-free variant will be kept as candidate waypoints for motion planning. When no collision-free variant is found, we slightly enlarge β by 10% and generate samples again. This step is repeated until a collision-free variant is found. Our motion planning algorithm will select one variant from the set of variants for each waypoint to form the final trajectory while considering the motion smoothness. Details will be presented in Section III-C.

B. Processing waypoints in singular region

By editing the orientations of the waypoints on a toolpath \mathcal{L} , we enhance its smoothness in MCS and also make it collision-free. However, the smoothness of \mathcal{L} in motion (particularly rotational axes) still needs to be further processed due to the singularity issue of $\text{atan2}()$ function used in IK.

Specifically, we define that a waypoint falls in the singular region \mathcal{R}_s if

$$\sqrt{(n_x/n_z)^2 + (n_y/n_z)^2} \leq \tan(\alpha). \quad (6)$$

Here α is a small threshold in angle relating to the machine's response speed on C-axis, and $\alpha = 4.5^\circ$ is used in our implementation according to experiment.

We are able to segment a given toolpath \mathcal{L} into the segments inside and out of singular region – denoted as \mathcal{L}_s and $\mathcal{L} \setminus \mathcal{L}_s$. The last singularity-free waypoint before entering \mathcal{R}_s (denoted by \mathbf{x}_s) and the first singularity-free waypoint after leaving \mathcal{R}_s (denoted by \mathbf{x}_e) are called *anchor* points as their orientations will *not* be processed. There are three different cases of \mathcal{L}_s including:

- 1) \mathcal{L}_s is connected with waypoints that are out of singular region in both sides,
- 2) \mathcal{L} ends with \mathcal{L}_s , and
- 3) \mathcal{L} starts from \mathcal{L}_s .

The last two are special cases of the first one, where singularity issue can be intuitively solved by aligning the orientation of all waypoints in \mathcal{L}_s to be the same as the orientation of anchor points \mathbf{x}_e or \mathbf{x}_s . In other words, B and C-axis motion are fixed for these special singular regions.

The singular region defined in Eq.(6) is inside a circle with radius as $\tan \alpha$ in the Cartesian coordinate system (as shown in the left of Fig. 6), which can also be represented as a band region as $B \in [-\alpha, +\alpha]$ by the cylindrical coordinates (as shown in the right of Fig. 6). For a general case of the toolpath portion \mathcal{L}_s in the singular region with two anchor waypoints \mathbf{x}_s and \mathbf{x}_e , we either push every waypoint to the boundary or make another path inside the singular region but with smaller angle change between neighboring waypoints.

The orientations of processed waypoints in \mathcal{L}_s should smoothly change between \mathbf{n}_s and \mathbf{n}_e , which are the orientations of \mathbf{x}_s and \mathbf{x}_e respectively. Assume C_s and C_e are the corresponding IK solution of \mathbf{x}_s and \mathbf{x}_e on C-axis and $\theta(C_e, C_s)$ returns the angle difference between them after

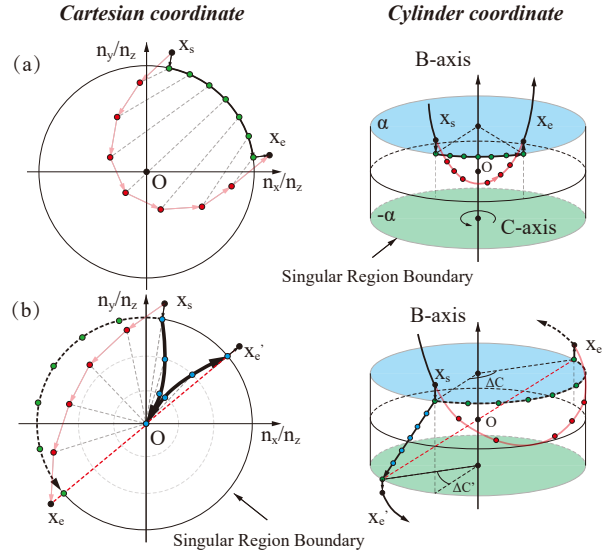


Fig. 6. Singularity processing for waypoints in \mathcal{L}_s . (a) Situation with $\Delta C = \|C_s - C_e\| < \frac{\pi}{2}$, pushing the waypoints $\mathbf{x} \in \mathcal{L}_s$ onto the boundary of the singular region. (b) By using the other feasible solution (denoted by \mathbf{x}'_e) for the anchor point \mathbf{x}_e , the waypoints $\mathbf{x} \in \mathcal{L}_s$ go through singular region orderly with less angle variation.

considering the winding effect, there are two cases when processing the waypoints in \mathcal{L}_s .

- $\theta(C_e, C_s) \leq \frac{\pi}{2}$: A minor arc is detected by projecting the anchor points, \mathbf{x}_s and \mathbf{x}_e , to the boundary of singular region. All waypoints in \mathcal{L}_s are projected onto this arc with equal distance. This ensures that the B-axis motion is locked (i.e., keeping a constant angle α) and C-axis has uniform and smooth motion within \mathcal{L}_s . An illustration of this projection can be found in Fig. 6(a).
- $\theta(C_e, C_s) > \frac{\pi}{2}$: The above method of projection can also be applied – see the black dash curve shown in the left of Fig. 6(b). However, a solution with smaller angle variation on C-axis can be found by using the other feasible solution of \mathbf{x}_e (denoted by \mathbf{x}'_e , which has an inverse value of B_e as $B'_e = -B_e$ and a value of C_e as $C'_e = C_e + \pi$). A newly updated toolpath \mathcal{L}_s can be obtained by generating an interpolation curve between (B_s, C_s) and (B'_e, C'_e) – see also the illustration in Fig. 6(b). This solution is better because of $\theta(C'_e, C_s) < \theta(C_e, C_s)$.

After applying this method to process the waypoints in \mathcal{L}_s , we can resolve the problem of large angle change on C-axis for most cases. However, there are still some extreme cases having too large angular change. We break toolpaths in these extreme regions although it rarely happens.

Changing orientations of the waypoints in \mathcal{L}_s will be possible to generate newly collided configurations. Specifically, if collision occurs at a waypoint $\bar{\mathbf{x}}_i$ processed from \mathbf{x}_i , the sampling method introduced in Section III-A is employed to generate k collision-free samples $\{\bar{\mathbf{x}}_i^j\}$ varied from $\bar{\mathbf{x}}_i$. To make the newly generated samples closer to $\bar{\mathbf{x}}_i$, the samples are generated within a smaller area (e.g., with the orientation change less than 10°). How to select samples to form the final motion trajectory will be discussed in the next sub-section.

ALGORITHM 1: Singularity-aware Motion Planning

Input: Waypoints for MAAM toolpath $\mathcal{L} = \{\mathbf{x}_0, \mathbf{x}_1 \dots \mathbf{x}_n\}$.
Output: The best feasible configurations for the waypoints on \mathcal{L} that give a collision-free and smooth motion.

```

/* Preprocessing */
1 Laplacian based smoothing for the orientations of waypoints;
/* Singularity-aware motion processing */
2 Run singularity check by Eq.(6) and detect the segment  $\mathcal{L}_s$ ;
3 Compute initial IK solution for all waypoints in  $\mathbb{R}_{MCS}^5$ ;
4 foreach  $\mathcal{L}_s = \{\mathbf{x}_s, \mathbf{x}_{s+1}, \dots, \mathbf{x}_e\}$  do
5   if  $\mathbf{x}_s = \mathbf{x}_0$  or  $\mathbf{x}_e = \mathbf{x}_n$  then
6     Fix B and C-axis motion with  $\mathbf{x}_s$  (or  $\mathbf{x}_e$ ).
7   else
8     /*  $\mathcal{L}_s$  in-and-out singular zone */
9     Generating new B- and C-axis coordinates for every
10    waypoints in  $\mathcal{L}_s$  by the method in Section III-B
11   end
12    $\forall \mathbf{x}_i \in \mathcal{L}_s$ , compute its singular-processed variant  $\bar{\mathbf{x}}_i$ ;
13 end
14 /* Generate collision-free variants */
15 foreach  $\mathbf{x}_i \in \mathcal{L}$  do
16   Run collision check for  $\mathbf{x}_i$  by Eq. 5;
17   if  $\Gamma(\mathbf{x}_i) > 0$  then
18     Generate  $k$  variants for  $\mathbf{x}_i$  outside the singular
19     region as  $\{\bar{\mathbf{x}}_i^j\}$ ;
20   end
21 end
22 /* Graph based search */
23 Construct  $\mathcal{G}$  by waypoints or their collision-free variants;
24 Apply the Dijkstra's algorithm to compute a shortest path  $\mathcal{T}$ 
25 on  $\mathcal{G}$  which minimizes  $J(\mathcal{T})$  defined in Eq.(7);
26 Compute X, Y, Z-axis coordinates for every nodes on  $\mathcal{T}$  by
27 IK solution (Table I);
28 return Optimized [X, Y, Z, B, C] of every nodes on  $\mathcal{T}$ .

```

C. Algorithms for Motion Planning

By applying the methods presented in the above two subsections, every waypoint $\mathbf{x}_i \in \mathcal{L}$ is in a status as one of the following three cases.

- *Case 1:* processed to a variant $\bar{\mathbf{x}}_i$ when \mathbf{x}_i falls in the singular region and $\bar{\mathbf{x}}_i$ is also collision-free;
- *Case 2:* processed into k collision-free variants $\{\bar{\mathbf{x}}_i^j\}$ if collision occurs at \mathbf{x}_i or collision happens at its variant $\bar{\mathbf{x}}_i$ with singularity processed;
- *Case 3:* kept unchanged when \mathbf{x}_i is neither in the singular region nor collided.

When applying IK computing, every waypoint \mathbf{x}_i (or its k variants) will be converted into 2 (or $2k$) feasible configurations $\{\mathbf{c}_i^a\}$ in MCS ($a = 1, 2$ or $a = 1, \dots, 2k$), where each configuration is treated as a sample for motion planning. The final trajectory of motion will be obtained by connecting one selected sample for every waypoints in \mathcal{L} .

A metric is defined as following to evaluate the rotational smoothness of a motion trajectory \mathcal{T}

$$J(\mathcal{T}) = \sum_i |B(\mathbf{c}_i^{T_i}) - B(\mathbf{c}_{i+1}^{T_{i+1}})| + |C(\mathbf{c}_i^{T_i}) - C(\mathbf{c}_{i+1}^{T_{i+1}})| \quad (7)$$

where T_i denotes the index of the selected sample for the trajectory \mathcal{T} at \mathbf{x}_i , and the coordinates of rotational axes for a configuration are given by $B(\cdot)$ and $C(\cdot)$. Here we use $L1$ -norm instead of $L2$ -norm here as $L1$ -norm is less sensitive to local errors. Note that although this metric only evaluates the angular change on B- and C-axes, it also indirectly measures

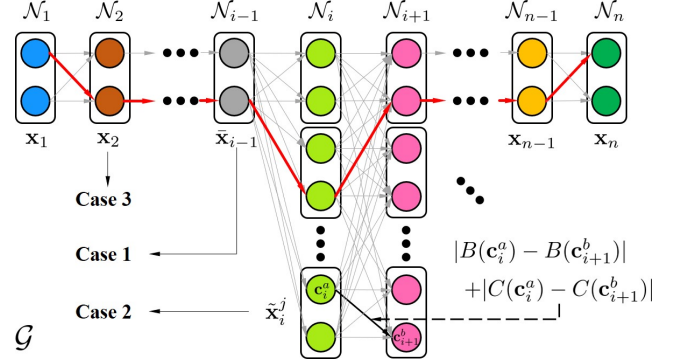


Fig. 7. A graph-based algorithm for searching a path (red) on which collision is eliminated and kinematics in singular region is optimized.

the smoothness of orientation change on the corresponding toolpath which is ensured by the mapping of forward kinematics. Among all possible trajectories, the ‘best’ one gives the smallest value of $J(\cdot)$.

A graph-based algorithm is employed to obtain the best trajectory. First of all, the samples of each waypoints in the machine configuration space MCS are converted into a column of 2 (or $2k$) nodes on a graph \mathcal{G} as each waypoint has two IK solutions based on Eqs.(3) and (4). The column of nodes for the waypoint \mathbf{x}_i is denoted by \mathcal{N}_i . For the toolpath \mathcal{L} with n waypoints, n columns of nodes are constructed (see Fig.7 for an illustration). Directed edges are added between nodes in neighboring columns. Specifically, for two nodes in two columns as $\mathbf{c}_i^a \in \mathcal{N}_i$ and $\mathbf{c}_{i+1}^b \in \mathcal{N}_{i+1}$, a directed edge pointing from \mathbf{c}_i^a to \mathbf{c}_{i+1}^b is added into \mathcal{G} with the weight of edge as $|B(\mathbf{c}_i^a) - B(\mathbf{c}_{i+1}^b)| + |C(\mathbf{c}_i^a) - C(\mathbf{c}_{i+1}^b)|$.

When construct the nodes of \mathcal{G} , collision is only considered and prevented at the samples of waypoints and their variants. Although rarely, collision can still occur when there is extremely large change of orientation between two neighboring nodes. To prevent this case, we compute the swept volume of a printer head between two waypoints [37] while constructing an edge between their corresponding nodes. If collision between this swept volume and the part of model already printed or the platform, we will remove this edge from the graph \mathcal{G} . As a result, all candidate paths on \mathcal{G} will be continuous collision-free. In our implementation, we compute the convex hull of printer head in two poses to approximate the general swept volume when the orientation change is small.

After constructing \mathcal{G} in the above way, the optimized trajectory of motion that minimize the objective function $J(\cdot)$ defined in Eq.(7) can be obtained by computing the shortest path on \mathcal{G} . The Dijkstra algorithm [38] is employed here. The pseudo-code for our singularity-aware motion planning is summarized in **Algorithm 1**. A collision-free trajectory with smooth motion can be obtained as the output of our method.

IV. EXPERIMENTAL RESULTS

We have implemented the motion planning pipeline for MAAM in C++. Source code of our implementation is released². Our method can be generally applied to all parallel multi-axis configurations as shown in Fig. 2, and a simulation

²https://github.com/zhangty019/MultiAxis_3DP_MotionPlanning

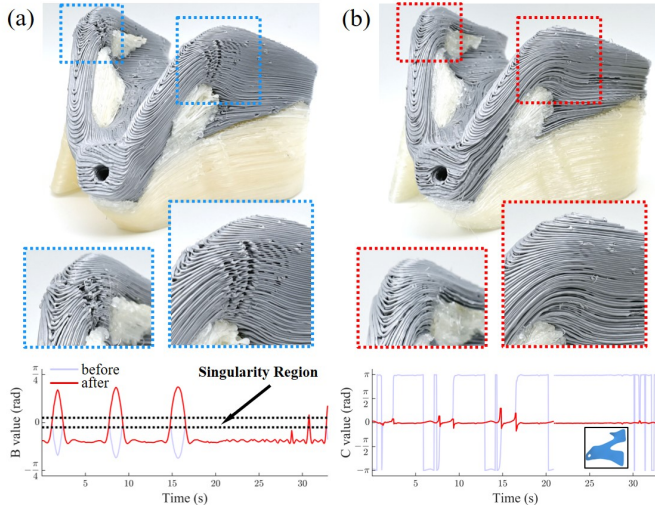


Fig. 8. Fabrication result for a mechanical model obtained from topology optimization – named as topo-opt. Artifacts that damage surface quality and break the continuity of filament can be found in the zoom view of (a), which is significantly reduced by applying our method – see the result shown in (b). The values of motion on B- and C-axes for a layer of toolpath are compared and given in two graphs at the bottom.

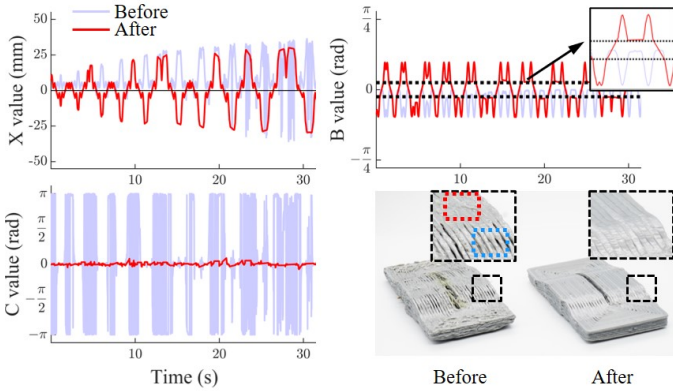
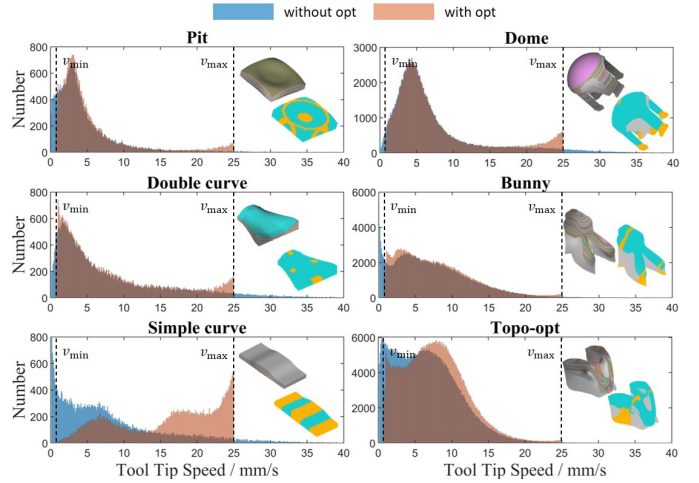


Fig. 9. The comparison of motion trajectories generated from orientation smoothed toolpaths, where the curves for the values on X-, B- and C-axes before vs. after applying our method are shown. The physically fabricated results shows that both over-extrusion (red rectangular) and under-extrusion (blue rectangular) can be effectively eliminated.

platform that can mimic the behavior of multi-axis motion is used to check collision before the physical fabrication (more details can be found in the Supplemental Video). The computation is efficient – e.g., the motion planning of toolpaths with $41k \sim 434k$ waypoints can be completed in $27.8 \sim 324.9$ sec. on a PC with 2.30GHz Intel Core i7-10875H CPU and 32GB memory. Experiment of fabrication has been conducted on different models to verify the effectiveness of our approach.

We first compare the results of models fabricated by using trajectories before and after applying our motion planning method. For the trajectory not optimized, it is also processed by Laplacian-based smoothing; but differently, the strategy of [20] is used in singular region by keeping the B- and C-angles unchanged in singular region and breaking the toolpath between waypoints having large angular variation. Two models, bunny and topo-opt, are tested and shown in Fig.1 and Fig.8 respectively. Significant quality improvement can be observed in the regions where toolpath falls into the singular region.



Model	without	with opt.	Model	without	with opt.
Pit	13.07%	2.90%	Dome	6.90%	1.48%
Double curve	11.99%	3.05%	Bunny	10.71%	2.03%
Simple curve	17.74%	0.14%	Topo-opt	9.28%	1.86%

Fig. 10. Histograms for the speed v of the tip of a printer head at all waypoints with vs. without singularity-aware optimization, where our tests are conducted on six different models with the singular waypoints displayed in yellow. Percentages of waypoints whose speed $v \notin [v_{\min}, v_{\max}]$ are reported in the table.

To quantitatively analyze the behavior of our method in enhancing the smoothness of axial motion, we visualize the values of B- and C-axes before and after applying our singularity-aware motion optimization in Fig. 8. The singular region has been given by dash lines, which is corresponding to the band region of cylindrical coordinate shown in Fig. 6. The motion has been optimized to require much less change on the C-axis between neighboring waypoints. The similar analysis is conducted for a model with relatively simpler shape (see the bottom row of Fig. 9), which however has a large area of surface falling in the singular region (i.e., with nearly vertical surface normal). For this example, we do not break a toolpath in singular region even for trajectory directly obtained from IK. Therefore, after generating over-extrusion in single region (see the region circled by red dash lines shown in Fig. 9), it is followed by a portion of under-extrusion that is caused by the hysteresis property of materials (see the region circled by blue dash lines). Both the over-extrusion and the under-extrusion can be eliminated on the result fabricated by using the motion trajectory optimized by our method. Note that the improvement of motion on C-axis is caused by the participate of motion on B-axis; therefore more significant movements occur on B-axis after optimization (see Figs. 8 and 9).

We have tested our method on a variety of models. It is found that our approach can effectively change the motion speed at the tip of a printer head to make it within the range of $[v_{\min}, v_{\max}]$. As shown in Fig. 10, the percentage of waypoints that violate this speed requirement can be significantly decreased after applying the optimization proposed in this paper. In our tests, $[v_{\min}, v_{\max}] = [1.0, 25.0]$ (mm/s) is employed according to the limited of feedrates that can be provided by the material extruder. Note that, the maximal speed of all motors on X-, Y-, Z-, B- and C-axes are considered when computing the feasible speed v on a machine here.

V. CONCLUSION AND FUTURE WORK

To support the manufacturing realization of designed tool-paths for MAAM in different machine configurations, we present a sampling-based motion planning method to solve the problems of singularity and collision in an integrated way. Variants with adjusted orientations are generated for waypoints when needed, and the best trajectory is obtained by connecting the IK solutions with minimal total change of angles on B- and C-axes. As a result, the motion therefore the quality of fabrication can be clearly improved, which has been demonstrated by experimental tests.

We have a few plans to further improve our approach in the future. During the optimization for singularity, the rotation of C-axis is assumed to be unlimited in the current formulation. However, for some machine configuration of MAAM (e.g., Fig. 2(b)), the motion on C-axis must be constrained due to the twining of electronic cables and material filaments. Constraints for this will be added in our future work. Besides the speed bounds of material extrusion, the acceleration and jerk limitation of actual material extrusion will be considered in our future work of motion planning.

REFERENCES

- [1] I. Gibson, D. W. Rosen, and B. Stucker, *Additive Manufacturing Technologies: Rapid Prototyping to Direct Digital Manufacturing*, 1st ed. Springer Publishing Company, Incorporated, 2009.
- [2] W. Gao, Y. Zhang, D. Ramanujan, K. Ramani, Y. Chen, C. B. Williams, C. C. Wang, Y. C. Shin, S. Zhang, and P. D. Zavattieri, "The status, challenges, and future of additive manufacturing in engineering," *Comput. Aided Des.*, vol. 69, pp. 65 – 89, 2015.
- [3] Y. Chen, C. Zhou, and J. Lao, "A layerless additive manufacturing process based on CNC accumulation," *Rapid Prototyping Journal*, vol. 17, pp. 218–227, 2011.
- [4] K. Hu, S. Jin, and C. C. L. Wang, "Support slimming for single material based additive manufacturing," *Comp. Aided Des.*, vol. 65, pp. 1–10, 2015.
- [5] J. Etienne, N. Ray, D. Panozzo, S. Hornus, C. C. L. Wang, J. Martínez, S. McMains, M. Alexa, B. Wyvill, and S. Lefebvre, "Curvislicer: Slightly curved slicing for 3-axis printers," *ACM Trans. Graph.*, vol. 38, no. 4, July 2019.
- [6] P. M. Bhatt, R. K. Malhan, P. Rajendran, and S. K. Gupta, "Building free-form thin shell parts using supportless extrusion-based additive manufacturing," *Additive Manufacturing*, vol. 32, p. 101003, 2020.
- [7] C. Dai, C. C. L. Wang, C. Wu, S. Lefebvre, G. Fang, and Y.-J. Liu, "Support-free volume printing by multi-axis motion," *ACM Trans. Graph.*, vol. 37, no. 4, July 2018.
- [8] C. Wu, C. Dai, G. Fang, Y.-J. Liu, and C. C. Wang, "General support-effective decomposition for multi-directional 3-d printing," *IEEE Trans. Auto. Sci. and Eng.*, vol. 17, pp. 599–610, 2020.
- [9] Y. Li, K. Tang, D. He, and X. Wang, "Multi-axis support-free printing of freeform parts with lattice infill structures," *Comput. Aided Des.*, vol. 133, p. 102986, 2021.
- [10] H. Peng, R. Wu, S. Marschner, and F. Guimbretière, "On-the-fly print: Incremental printing while modelling," in *Proceedings of the 2016 CHI Conference on Human Factors in Computing Systems*, 2016, p. 887–896.
- [11] W. Wang, Y.-J. Liu, J. Wu, S. Tian, C. C. L. Wang, L. Liu, and X. Liu, "Support-free hollowing," *IEEE Trans. Visualization and Computer Graphics*, vol. 24, no. 10, pp. 2787–2798, 2018.
- [12] H. Zhang, D. Liu, T. Huang, Q. Hu, and H. Lammer, "Three-dimensional printing of continuous flax fiber-reinforced thermoplastic composites by five-axis machine," *Materials*, vol. 13, no. 7, 2020.
- [13] G. Fang, T. Zhang, S. Zhong, X. Chen, Z. Zhong, and C. C. L. Wang, "Reinforced fdm: Multi-axis filament alignment with controlled anisotropic strength," *ACM Trans. Graph.*, vol. 39, no. 6, Nov. 2020.
- [14] M. A. Isa and I. Lazoglu, "Five-axis additive manufacturing of freeform models through buildup of transition layers," *Int. Journal of Manufacturing Systems*, vol. 50, pp. 69 – 80, 2019.
- [15] F. Wulle, D. Coupek, F. Schöffner, A. Verl, F. Oberhofer, and T. Maier, "Workpiece and machine design in additive manufacturing for multi-axis fused deposition modeling," *Procedia CIRP*, vol. 60, pp. 229–234, 2017.
- [16] S. Gantenbein, K. Masania, W. Woigk, J. P. Sesseg, T. A. Tervoort, and A. R. Studart, "Three-dimensional printing of hierarchical liquid-crystal-polymer structures," *Nature*, vol. 561, pp. 226–230, 2018.
- [17] Z. Lin, J. Fu, H. Shen, and W. Gan, "Non-singular tool path planning by translating tool orientations in c-space," *The International Journal of Advanced Manufacturing Technology*, vol. 71, no. 9, pp. 1835–1848, Apr 2014.
- [18] A. Affouard, E. Duc, C. Lartigue, J.-M. Langeron, and P. Bourdet, "Avoiding 5-axis singularities using tool path deformation," *Int. Journal of Machine Tools and Manufacture*, vol. 44, no. 4, pp. 415 – 425, 2004.
- [19] K. Sørby, "Inverse kinematics of five-axis machines near singular configurations," *Int. Journal of Machine Tools and Manufacture*, vol. 47, no. 2, pp. 299 – 306, 2007.
- [20] Y. Jung, D. Lee, J. Kim, and H. Mok, "Nc post-processor for 5-axis milling machine of table-rotating/tilting type," *Journal of Materials Proc. Tech.*, vol. 130-131, pp. 641–646, 2002, aFDM 2002 S.I.
- [21] Y. Boz and I. Lazoglu, "A postprocessor for table-tilting type five-axis machine tool based on generalized kinematics with variable feedrate implementation," *The International Journal of Advanced Manufacturing Technology*, vol. 66, no. 9, pp. 1285–1293, Jun 2013.
- [22] J. Yang and Y. Altintas, "Generalized kinematics of five-axis serial machines with non-singular tool path generation," *Int. Journal of Machine Tools and Manufacture*, vol. 75, pp. 119–132, 2013.
- [23] C. A. My and E. L. Bohez, "New algorithm to minimise kinematic tool path errors around 5-axis machining singular points," *Int. Journal of Production Research*, vol. 54, no. 20, pp. 5965–5975, 2016.
- [24] L. Grandguillaume, S. Lavernhe, and C. Tournier, "Kinematical smoothing of rotary axis near singularity point," *Materials Science Forum*, vol. 836-837, 10 2015.
- [25] N. Wang and K. Tang, "Automatic generation of gouge-free and angular-velocity-compliant five-axis toolpath," *Comput. Aided Des.*, vol. 39, no. 10, pp. 841 – 852, 2007.
- [26] V. Lacharnay, S. Lavernhe, C. Tournier, and C. Lartigue, "A physically-based model for global collision avoidance in 5-axis point milling," *Comput. Aided Des.*, vol. 64, pp. 1 – 8, 2015.
- [27] J. Xu, D. Zhang, and Y. Sun, "Kinematics performance oriented smoothing method to plan tool orientations for 5-axis ball-end CNC machining," *Int. Journal of Mech. Sci.*, vol. 157-158, pp. 293 – 303, 2019.
- [28] S. Hornus, T. Kuipers, O. Devillers, M. Teillaud, J. Martínez, M. Glisse, S. Lazard, and S. Lefebvre, "Variable-width contouring for additive manufacturing," *ACM Trans. Graph.*, vol. 39, no. 4, July 2020.
- [29] T. Kuipers, E. L. Doubrovski, J. Wu, and C. C. L. Wang, "A framework for adaptive width control of dense contour-parallel toolpaths in fused deposition modeling," *Comput. Aided Des.*, vol. 128, p. 102907, 2020.
- [30] H. Zhao, F. Gu, Q.-X. Huang, J. Garcia, Y. Chen, C. Tu, B. Benes, H. Zhang, D. Cohen-Or, and B. Chen, "Connected fermat spirals for layered fabrication," *ACM Trans. Graph.*, vol. 35, no. 4, 2016.
- [31] J. Jiang and Y. Ma, "Path planning strategies to optimize accuracy, quality, build time and material use in additive manufacturing: A review," *Micromachines*, vol. 11, no. 7, 2020.
- [32] P. M. Bhatt, R. K. Malhan, A. V. Shembekar, Y. J. Yoon, and S. K. Gupta, "Expanding capabilities of additive manufacturing through use of robotics technologies: A survey," *Additive Manufacturing*, vol. 31, p. 100933, 2020.
- [33] F. Xie, L. Chen, Z. Li, and K. Tang, "Path smoothing and feed rate planning for robotic curved layer additive manufacturing," *Robotics and Computer-Integrated Manufacturing*, vol. 65, p. 101967, 2020.
- [34] A. V. Shembekar, Y. J. Yoon, A. Kanyuck, and S. K. Gupta, "Generating robot trajectories for conformal three-dimensional printing using nonplanar layers," *Journal of Computing and Information Science in Engineering*, vol. 19, no. 3, 04 2019.
- [35] Y. Huang, J. Zhang, X. Hu, G. Song, Z. Liu, L. Yu, and L. Liu, "Framefab: Robotic fabrication of frame shapes," *ACM Transactions on Graphics*, vol. 35, 2016.
- [36] C. Dai, S. Lefebvre, K. M. Yu, J. M. P. Geraedts, and C. C. L. Wang, "Planning jerk-optimized trajectory with discrete time constraints for redundant robots," *IEEE Trans. Auto. Sci. and Eng.*, vol. 17, no. 4, pp. 1711–1724, 2020.
- [37] Y. J. Kim, G. Varadhan, M. C. Lin, and D. Manocha, "Fast swept volume approximation of complex polyhedral models," *Comput. Aided Des.*, vol. 36, pp. 1013–1027, 2004.
- [38] E. W. Dijkstra, "A note on two problems in connexion with graphs," *Numerische Mathematik*, vol. 1, pp. 269–271, 1959.